PNAS RESEARCH ARTICLE | NEUROSCIENCE OPEN ACCESS

Plasticity of thalamocortical axons is regulated by serotonin levels modulated by preterm birth

Alexander Sinclair-Wilson[a], Akindé Lawrence[a], Isabelle Ferezou[b], Hugues Cartonnet[a], Caroline Mailhes[c], Sonia Garel[a,d,1,2], and Ludmilla Lokmane[a,1,2]

Edited by Carol Mason, Columbia University, New York, NY; received January 31, 2023; accepted July 9, 2023

Sensory inputs are conveyed to distinct primary areas of the neocortex through specific thalamocortical axons (TCA). While TCA have the ability to reorient postnatally to rescue embryonic mistargeting and target proper modality-specific areas, how this remarkable adaptive process is regulated remains largely unknown. Here, using a mutant mouse model with a shifted TCA trajectory during embryogenesis, we demonstrated that TCA rewiring occurs during a short postnatal time window, preceded by a prenatal apoptosis of thalamic neurons—two processes that together lead to the formation of properly innervated albeit reduced primary sensory areas. We furthermore showed that preterm birth, through serotonin modulation, impairs early postnatal TCA plasticity, as well as the subsequent delineation of cortical area boundary. Our study defines a birth and serotonin-sensitive period that enables concerted adaptations of TCA to primary cortical areas with major implications for our understanding of brain wiring in physiological and preterm conditions.

thalamic axons | plasticity | preterm birth | serotonin | sensitive period

Significance

Brain functioning relies on circuits that begin to assemble prenatally and are remodeled during postnatal life. In particular, sensory information is conveyed to cortical areas via thalamocortical axons (TCA), which are shaped by embryonic guidance and postnatal plasticity. Elucidating the mechanisms underlying TCA wiring is critical for our understanding of sensory circuit development. Here, we revealed the existence of a short time window of plasticity that supports the correction of TCA embryonic mistargeting. We furthermore show that this period is sensitive to serotonin levels, which are modulated by preterm birth. Our study highlights a birth and serotonin-sensitive period of plasticity, key for the rescue of prenatal miswiring, thereby providing insights into physiological and pathological brain wiring.

Brain functioning relies on neuronal circuits formed through a dynamic interplay between developmental programs, activity, and other processes, such as birth. While our understanding of the role of these interplays in the emergence of functional circuits has considerably advanced (1–5), there is a paucity of data on how the timing of birth and early associated perturbations may impact adaptive plasticity of brain circuits. This issue is important since early preterm birth or early-life perturbations have been shown to constitute risk factors for several neurodevelopmental disorders (6–8).

In mammals, the cerebral cortex is subdivided into functional areas, each characterized by a stereotypical pattern of gene expression and cytoarchitecture, as well as reciprocal connectivity with specific thalamic nuclei (1, 9, 10). In particular, the primary visual (V1) and somatosensory (S1) areas receive sensory input directly from primary, or first-order, modality-specific thalamic nuclei: the dorsal lateral geniculate (dLGN), and the ventral posterior (VP), respectively (1, 9, 11–13). The formation of these circuits relies on sequentially orchestrated processes. First, embryonic thalamocortical axons (TCA) navigate through an intermediate target, the subpallium, in which they are organized and directed to their presumptive target areas (14–22). Second, after a waiting period in the subplate, TCA perinatally invade cortical layers (3, 23). Third, postnatally, TCA substantially contribute to the ongoing arealization process by influencing cortical neurons and elaborating cortical maps such as the barrel field in S1 corresponding to the map of rodent snout whiskers (19, 24–26).

Over the past decade, the understanding of the mechanisms regulating TCA guidance and the formation of functional sensory maps has been considerably advanced through studies in mice (25–27). Initial gradients of morphogens, transcription factors, and guidance molecules shape protomaps and thalamic nuclei, as well as guide TCA through the subpallium before their tight and regulated interactions with the subplate during the waiting period (3, 4, 23, 28). In addition, thalamic neuronal activity prenatally (29–32) and postnatally has respectively been shown to shape the size of S1 and to pattern sensory maps (3, 25, 26, 33–37). On a different scale, the timing of birth modulates the kinetics of cortical sensory map development (38). Indeed, preterm birth induced in mice accelerates the kinetics of barrel field formation due to a precipitated decrease in the levels of the neuromodulator serotonin (5-hydroxytryptamine, 5-HT) (38), a known regulator of TCA growth and sensory map formation (39–46).

The step-by-step guidance of TCA is also related to their remarkable ability to adapt and rewire, and these processes modulate the formation of cortical areas and sensory maps. In particular, TCA innervation modulates cortical sensory representation, as selective reduction or elimination of primary thalamic nuclei (VP or dLGN) triggers corresponding adaptive changes in primary sensory areas at the expense of neighboring higher-order

Author contributions: A.S.-W., I.F., S.G., and L.L. designed research; A.S.-W., A.L., I.F., H.C., C.M., and L.L. performed research; A.S.-W., A.L., I.F., H.C., S.G., and L.L. analyzed data; and A.S.-W., S.G., and L.L. wrote the paper.

The authors declare no competing interest.

This article is a PNAS Direct Submission.

[1]S.G. and L.L. contributed equally to this work.

[2]To whom correspondence may be addressed. Email: garel@bio.ens.psl.eu or lokmane@bio.ens.psl.eu.

This article contains supporting information online at https://www.pnas.org/lookup/suppl/doi:10.1073/pnas.2301644120/-/DCSupplemental.

Published August 7, 2023.

(HO) regions involved in integrative and cognitive processes (47–50). In addition, TCA exhibit long-range adaptive plasticity during early postnatal life (14, 16, 51, 52). For example, embryonic TCA mistargeting (14, 51) or defective cortical regionalization (52), both of which lead to the innervation of inappropriate cortical targets, are rescued after birth, allowing TCA to match their target modality-specific cortical areas. Yet, the time window that supports this remarkable postnatal cross-areal plasticity and its underlying mechanisms remain largely unexplored.

Here, we investigate this issue by taking advantage of a powerful genetic mouse model, *Ebf1*cKO, in which we showed that embryonic TCA mistargeting was corrected by a postnatal readdressing of axons to their proper cortical areas (14). We show that this remarkable TCA adaptation occurs during a short and discrete postnatal period and is perturbed by a premature birth through a serotonin-dependent process, thus impacting cortical arealization. Our findings reveal a plasticity period following birth that relies on serotonin, with significant implications for our understanding of the mechanisms controlling TCA wiring and the emergence of cortical areas as well as of the detrimental effects of preterm birth.

Results

Rewiring of Mistargeted TCA Occurs during a Short Postnatal Time Window. To study the events associated with the postnatal rewiring of TCA to the corresponding cortical target areas, we used conditional *Dlx5/6::cre; Ebf1*$^{fl/-}$ mice (*Ebf1*cKO), a powerful genetic model (14, 53). This mutation disrupts the development of the subpallium without affecting the prenatal cortical or thalamic patterning (14), as supported by the expression of molecular markers of specific thalamic nuclei (50) (*SI Appendix*, Fig. S1). Consequently, this mutation nonautonomously disrupts the embryonic pathfinding of TCA through the subpallium, as illustrated by Netrin-G1 (NetG1) immunostainings, which label TCA (Fig. 1*A*). Using carbocyanine dye injections at embryonic day (E) 17.5 to label TCA from specific thalamic nuclei, we found ventrally misrouted TCA include visual-dLGN axons (Fig. 1*A*). Retrolabeling using carbocyanine dye in specific cortical areas showed that visual-dLGN axons did not reach the presumptive V1 at birth, while some somatosensory–VP axons were caudally shifted, invading V1 instead of S1 (Fig. 1*A* and refer to *Materials and Methods* for details on dye positioning/injections) (14). Since we previously showed that such early defects could be rescued by postnatal day (P) P7 (14), we investigated the precise time course of events underlying this remarkable plasticity.

We first performed a longitudinal study of apoptosis using cleaved caspase 3 (cCasp3) immunostaining that revealed a massive cell death specifically at E17.5, in the dLGN and VP thalamic nuclei of mutants (Fig. 1*B*). Notably, negligible apoptosis was observed postnatally or in other thalamic nuclei, including in HO somatosensory (POm, posteromedial nucleus) and visual (LP, lateral posterior nucleus) thalamic nuclei, as delineated by a panel of molecular markers (*SI Appendix*, Fig. S2 *A* and *B*). Accordingly, we observed a reduction in the global size of the thalamus, and coherently, VP and dLGN nuclei were selectively reduced in mutants compared to controls (*SI Appendix*, Fig. S2*C*). Since the size of thalamic nuclei defines the size of the corresponding primary cortical areas (47–49), we examined cortical area maps at P7, including V1, S1, and the interposed HO posterior parietal association area (PTLp, also known as PPC for posterior parietal cortex) (54, 55). Using TCA markers, including the TCA-GFP line (56), 5-HTT, and vGlut2, as well as the expression of cortical markers *Rorβ* and *Lmo4* (48, 57, 58) (Fig. 1*C* and *SI Appendix*, Fig. S3*A*), we observed that while the cortical surface remained unchanged (Fig. 1 *C* and *D* and *SI Appendix*, Fig. S3*A*), the size of V1 and S1 was significantly reduced in mutant mice, at the expense of an increase in the size of HO PTLp, located between V1 and S1 (Fig. 1 *C* and *D*). This relative change in the size of cortical areas occurred without modifying their relative positioning or the localization of the caudal border of S1 (*SI Appendix*, Fig. S3*B*). In addition, primary cortical areas still responded to specific sensory modalities in adult *Ebf1*cKO mice (59, 60), since visual stimulation or whisker deflection triggered a focal, albeit reduced, activity pattern within the corresponding V1 and S1 (*SI Appendix*, Fig. S3*C*). Thus, embryonic TCA misrouting and rescue led to the formation of reduced but well-defined and functional primary cortical areas, which raised the question of the timing of axonal rewiring.

We performed axonal tracing experiments at successive postnatal stages (Fig. 1*E*) and established a "matching index" to quantify TCA mistargeting and plasticity (Fig. 1*F*). This index evaluates the innervation of V1 by visual thalamic axons by measuring the percentage of retrolabeled cells in visual thalamic nuclei (dLGN and VP) relative to all thalamic retrolabeling including somatosensory nuclei (VP and POm) after a DiI injection into V1 (*SI Appendix*, Fig. S3 *D* and *E*, refer to *Materials and Methods*). At P0, when ventrally misrouted dLGN axons do not reach V1, the matching index was very low in mutant pups (Fig. 1 *A* and *F*), while we began to observe TCA rewiring from P1 (Fig. 1 *E* and *F*), with substantial rewiring occurring by P2 in mutants (Fig. 1 *E* and *F*). Indeed, DiI/DiA double injections in P2 *Ebf1*cKO showed an exclusive retrolabeling of dLGN neurons from V1 and lateral retrolabeling of VP neurons from S1, which was similar to that observed in control animals (Fig. 1 *E* and *F*). In addition, some of the dLGN axons that finally reached V1 were initially misrouted in the subpallium, as indicated by their axonal trajectory (Fig. 1*E*). Taken together, these experiments revealed that after a first prenatal impact on the survival of thalamic nuclei, TCA miswiring is followed by a rapid postnatal rewiring at P1, which enables subsequent matching of TCA to their respective cortical targets, starting from P2 (Fig. 1*G*).

Postnatal Plasticity Is Impaired by Preterm Birth. Critical events after birth, including changes in sensory stimulation and subcortical inputs, have been shown to shape the formation of the cortical barrel map (24, 26). Thus, we hypothesized that birth may be involved in the temporal regulation of this short postnatal window, during which TCA rewiring occurs. Since emerging activity from the whisker pad increases at birth, we first performed infraorbital nerve (ION) sectioning from birth to dampen the activity coming from the whisker pad, a procedure known to disrupt TCA activity and their aggregation in the barrel field (19, 24). We observed a comparable pattern of axonal tracing in ION-sectioned and untreated (unsectioned) mutants at P7, demonstrating that TCA plasticity in *Ebf1*cKO is independent of peripheral activity (*SI Appendix*, Fig. S4 *A* and *B*).

Next, to directly test the role of the timing of birth in TCA plasticity, we induced preterm parturition (PT) by administrating mifepristone, a progesterone receptor antagonist, to pregnant mice at E17.5 (38, 61), thus triggering delivery and birth 1 d before term (Fig. 2*A*). As previously shown (38), we observed that preterm birth accelerated the formation of TCA clusters in the barrel field (Fig. 2 *B* and *C*). Indeed, in untreated full-term conditions, we used the TCA-GFP line (Fig. 2*B*) or vGlut2 staining (*SI Appendix*, Fig. S4*C*) and observed a rapid onset of TCA clustering after birth between P2 and P3 (Fig. 2*B*), with an increase in the "barrel field formation index" (Fig. 2*C*), quantified as described in ref. 38. In the PT condition, the analysis revealed that barrel field formation was

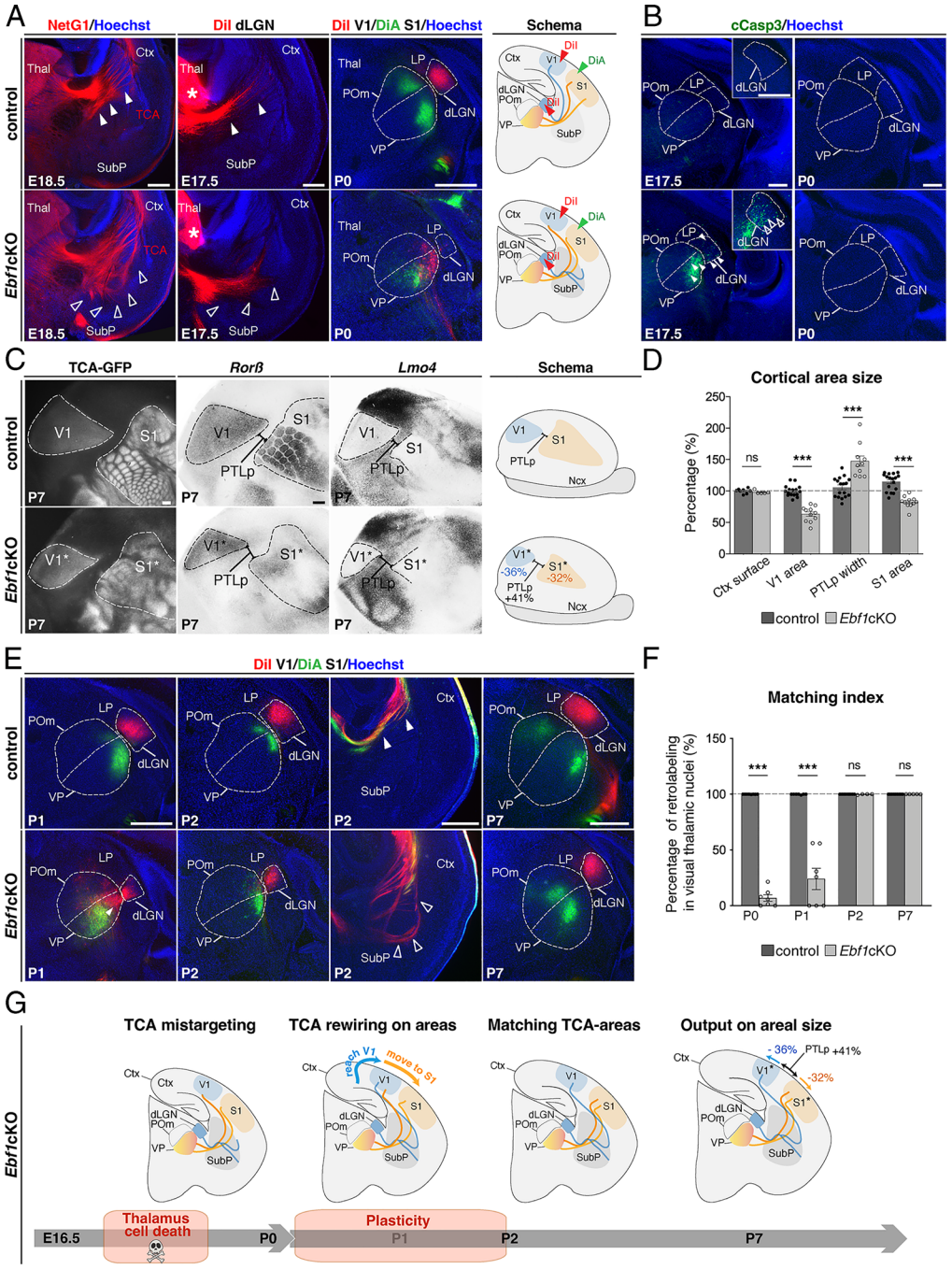

Fig. 1. Embryonic TCA mistargeting is rapidly corrected after birth. (*A*) NetG1 staining on the coronal section of E18.5 ($n_{control}$ = 4; n_{mutant} = 4) showing the abnormal pathfinding of TCA in the subpallium (open arrowheads) in *Ebf1*cKO (*Dlx5/6::Cre;Ebf1*$^{fl/-}$) compared to control (solid arrowheads) embryos. Coronal section of the subpallium at E17.5 after DiI injections in the dLGN ($n_{control}$ = 7; n_{mutant} = 6) indicating that dLGN TCA are misrouted in the ventral subpallium in *Ebf1*cKO (open arrowheads) compared to control (solid arrowheads) embryos. Coronal section of the thalamus after DiI injection into V1 (red) and DiA injection into caudal S1 (green) in control (n = 8) and *Ebf1*cKO (n = 7) mice, demonstrating that TCA target inappropriate cortical domains at P0. Schematic representation of DiI/DiA placements as well as aberrant TCA pathfinding through the mutant subpallium compared to controls. (*B*) Cleaved caspase-3 staining (cCasp3) on the coronal section, revealing massive apoptosis in the VP thalamic nucleus (solid arrowheads) and the dLGN at a more rostral level (*Inset*, open arrowheads) in E17.5 *Ebf1*cKO (n = 4) compared to control (n = 3) embryos, while limited staining was observed in both conditions at P0 ($n_{control}$ = 4; n_{mutant} = 4). (*C*) TCA-GFP ($n_{control}$ = 10; n_{mutant} = 9) staining and in situ hybridization of specific cortical markers *Rorβ* and *Lmo4* (at least n = 5 for each condition) on the P7 flattened cortex showing a severe reduction of V1 and S1 areas (dotted lines delineation) at the expense of the intercalated HO PTLp domain in *Ebf1*cKO mice: −32% for S1; −36% for V1 and +41% for the PTLp domain. (*D*) Quantification of the size of the cortical surface (control = 100 ± 1.34%, n = 8; mutant = 98.03 ± 1.25%, n = 5), V1 area (control = 100 ± 2.20%, n = 16; mutant = 63.30 ± 3.64%, n = 11), S1 area (control = 114.7 ± 3.30%, n = 17; mutant = 82.49 ± 2.71%, n = 11) and PTLp width (control = 105.7 ± 3.86%, n = 17; mutant = 147.40 ± 8.40%, n = 11) at P7. (*E*) Coronal section of the thalamus at P1, P2, and P7 and of the subpallium at P2 after DiI injection into V1 (red) and DiA injection into caudal S1 (green) showing rapid TCA rewiring after birth with some ventrally misrouted dLGN TCA reaching V1 in *Ebf1*cKO (open arrowheads) compared to control (solid arrowheads) mice. (*F*) Quantification of the matching index (as defined in *SI Appendix*, Fig. S3*B*) by measuring the proportion of the red signal in visual thalamic nuclei (dLGN and LP) following DiI injection into V1. $P0_{control}$ = 99.95 ± 0.03% (n = 8) vs. $P0_{mutant}$ = 6.89 ± 2.95% (n = 7); $P1_{control}$ = 99.89 ± 0.11% (n = 7) vs. $P1_{mutant}$ = 24.05 ± 9.53% (n = 7); $P2_{control}$ = 99.99 ± 0.01% (n = 8) vs. $P2_{mutant}$ = 99.82 ± 0.17% (n = 4); $P7_{control}$ = 99.99 ± 0.01% (n = 9) vs. $P7_{mutant}$ = 99.97 ± 0.02% (n = 5). (*G*) Sequential events enabling postnatal TCA plasticity in *Ebf1*cKO mice and subsequent impact on the primary cortical areas. Values are presented as mean ± SEM; ***P < 0.001, Mann–Whitney U test for *D* and two-way ANOVA with Sidak's correction for multiple comparisons for *F* (Scale bars, 250 μm). Ctx, cortex; dLGN, dorsal lateral geniculate nucleus; LP, lateral posterior nucleus; POm, posteromedial nucleus; PTLp, posterior parietal association area; S1, primary somatosensory cortex; SubP, subpallium; Thal, thalamus; V1, primary visual cortex; VP, ventroposterior nucleus. See also *SI Appendix*, Figs. S1–S3 and S8.

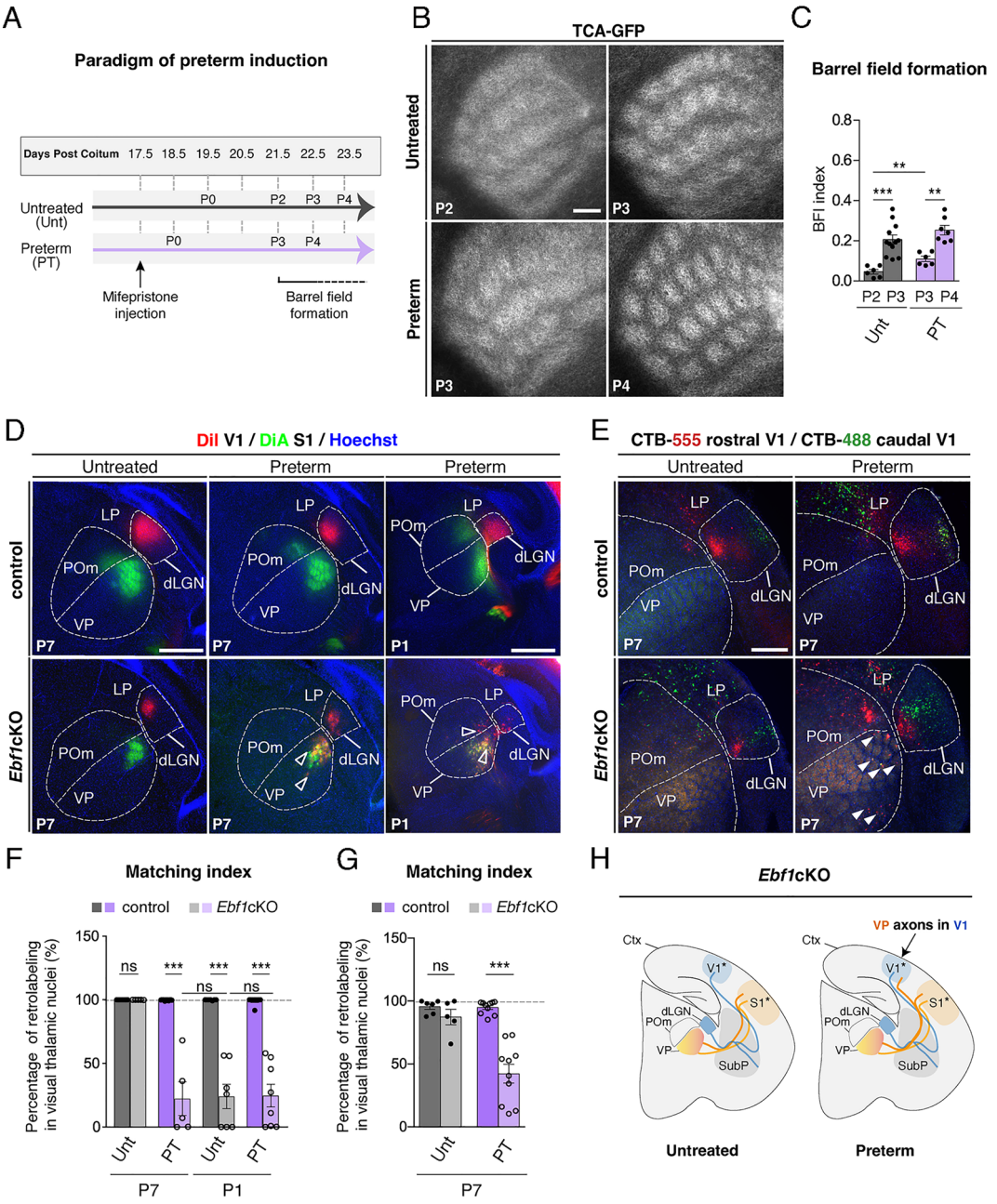

Fig. 2. Preterm birth affects the efficiency of TCA rewiring. (*A*) Experimental procedure to induce preterm birth using mifepristone injection at E17.5. (*B*) TCA-GFP immunostaining on the flattened cortex of P2 to P3 untreated (full-term) and P3 to P4 preterm pups. (*C*) Barrel filed formation, quantified as the Barrel Field Intensity (BFI) index using the TCA-GFP line, increases in the postnatal stages: $Untreated_{P2}$ = 0.047 ± 0.011% (n = 6) vs. $Untreated_{P3}$ = 0.210 ± 0.023% (n = 12) or $Preterm_{P3}$ = 0.11 ± 0.013% (n = 6) and $Preterm_{P3}$ vs. $Preterm_{P4}$ = 0.25 ± 0.024% (n = 7). (*D*) Coronal section of the thalamus after DiI injection into V1 (red) and DiA injection into caudal S1 (green) in control and *Ebf1*cKO (*Dlx5/6::Cre;Ebf1*$^{fl-/-}$) mice in the P7 untreated, P7 preterm, and P1 preterm conditions. In preterm *Ebf1*cKO at P7 and P1, V1 injection (red) simultaneously led to a retrolabeling in the VP and dLGN thalamic nuclei, indicating that some TCA of the VP nucleus targeted V1 instead of S1 (empty arrowheads). (*E*) Coronal section of the thalamus after CTB-555 injection into rostral V1 (red) and CTB-488 injection into caudal V1 (green) in control and *Ebf1*cKO mice at P7 in the untreated and preterm conditions. V1 double injections in preterm *Ebf1*cKO mice reveal the defective plasticity of TCA as shown by retrolabeling in the somatosensory-VP nuclei (arrowheads). (*F*) Quantification of the matching index by measuring the proportion of the red signal in visual thalamic nuclei (dLGN and LP) following DiI injection into V1 for *D*. At P7: $Untreated_{control}$ = 99.99 ± 0.002% (n = 9) vs. $Untreated_{mutant}$ = 99.97 ± 0.02% (n = 5); $Preterm_{control}$ = 99.73 ± 0.12% (n = 12) vs. $Preterm_{mutant}$ = 22.32 ± 13.23% (n = 5). At P1: $Untreated_{control}$ = 99.89 ± 0.11% (n = 7) vs. $Untreated_{mutant}$ = 24.05 ± 9.53% (n = 7); $Preterm_{control}$ = 98.96 ± 1.03% (n = 8) vs. $Preterm_{mutant}$ = 24.74 ± 8.80% (n = 8). (*G*) Quantification of the matching index at P7 by measuring the proportion of the signal in visual thalamic nuclei (dLGN and LP) following CTB injection into V1 for *E*. $Untreated_{control}$ = 95.51 ± 2.18% (n = 6) vs. $Untreated_{mutant}$ = 87.22 ± 6.12% (n = 5); $Preterm_{control}$ = 94.85 ± 1.61% (n = 10) vs. $Preterm_{mutant}$ = 42.25 ± 7.39% (n = 10). (*H*) Defective TCA plasticity in preterm *Ebf1*cKO at P7 as V1 was targeted by dLGN and some VP axons. Values are presented as mean ± SEM; $^{**}P < 0.01$, $^{***}P < 0.001$, Mann–Whitney *U* test for *C* and two-way ANOVA with Sidak's correction for multiple comparisons for *F* and *G* (Scale bars, 250 μm). Ctx, cortex; dLGN, dorsal lateral geniculate nucleus; LP, lateral posterior nucleus; POm, posteromedial nucleus; S1, primary somatosensory cortex; SubP, subpallium; V1, primary visual cortex; VP, ventroposterior nucleus. See also *SI Appendix*, Figs. S4, S5, and S8.

accelerated at the corresponding developmental stages P3 and P4, with a higher axonal clustering in P3 PT compared to P2 untreated pups (Fig. 2 *B* and *C*). We next performed axonal tracing through cortical DiI/DiA injections into V1 and S1, respectively, in untreated and PT *Ebf1*cKO conditions at P7 (Fig. 2*D*). As expected, in untreated mutants, TCA rewiring was fully efficient, highlighted by exclusive retrolabeling of dLGN neurons after V1 DiI injections and of VP neurons after S1 DiA injections (Figs. 1 *E* and *G* and 2 *D* and *F*). However, PT birth notably affected the efficiency of TCA plasticity in *Ebf1*cKO. Indeed, in PT *Ebf1*cKO, we found that DiI

injection into V1 retrolabeled neurons located in both the dLGN and VP nuclei (Fig. 2 *D* and *F*) indicating that a portion of the somatosensory-VP axons was still lagging in V1 (Fig. 2*H*). Furthermore, this impairment was present since P1 (Fig. 2*D*), suggesting that TCA rewiring began after birth but ended prematurely in PT *Ebf1*cKO pups (Fig. 2 *D* and *F*). To validate axonal populations innervating V1, we also performed in vivo double injections of CTB retrograde tracers into V1 (Cholera Toxin Subunit-B), which leads to a much more focal labeling than dye tracing (62) (*SI Appendix*, Fig. S4*D*). In PT *Ebf1*cKO, compared to PT control or untreated mutant, we still observed retrolabeling of both dLGN and VP neurons, confirming that both TCA subsets target V1 at P7 (Fig. 2 *E* and *G*). Overall, our results indicate that preterm birth alters TCA plasticity during a sensitive early postnatal time window, resulting in the persistence of mistargeted VP axons in V1 (Fig. 2*H*).

TCA Plasticity Relies on Birth-Dependent Modulation of 5-HT. It has been previously established that PT induces a premature decrease in the levels of 5-HT (38), which prompted us to explore the role of 5-HT in TCA plasticity. We hypothesized that the extraordinary axonal rewiring observed in the *Ebf1*cKO model might be dependent on a certain level of 5-HT during the short postnatal window of plasticity. Thus, a reduction in 5-HT levels upon the induction of PT may contribute to TCA plasticity deficits in *Ebf1*cKO animals. We investigated the effect of 5-HT in *Ebf1*cKO during the plasticity window by performing either i) a pharmacological reduction in 5-HT levels through daily injections of parachlorophenylalanine (PCPA, P0 to P3), a 5-HT synthesis inhibitor (38, 41), or ii) a pharmacological increase in 5-HT levels in the PT condition through daily injections of fluoxetine (Fx, P0 to P3), a selective serotonin reuptake inhibitor (SSRI) used for the treatment of depression (63, 64) (Fig. 3*A*). Notably, the two treatments had no additional impact on the size of thalamic nuclei in either mutants or controls (*SI Appendix*, Fig. S5*B*). By performing axonal tracing at P7 with cortical DiI/DiA injections, we first observed that modulating 5-HT levels after birth in control conditions had no effect on cortical TCA targeting (Fig. 3 *B* and *C*). In contrast, induced reduction in 5-HT levels in *Ebf1*cKO mutants since birth partially recapitulated TCA plasticity defects observed in the PT condition (Fig. 3 *B* and *C*). Conversely, increasing 5-HT levels in PT *Ebf1*cKO

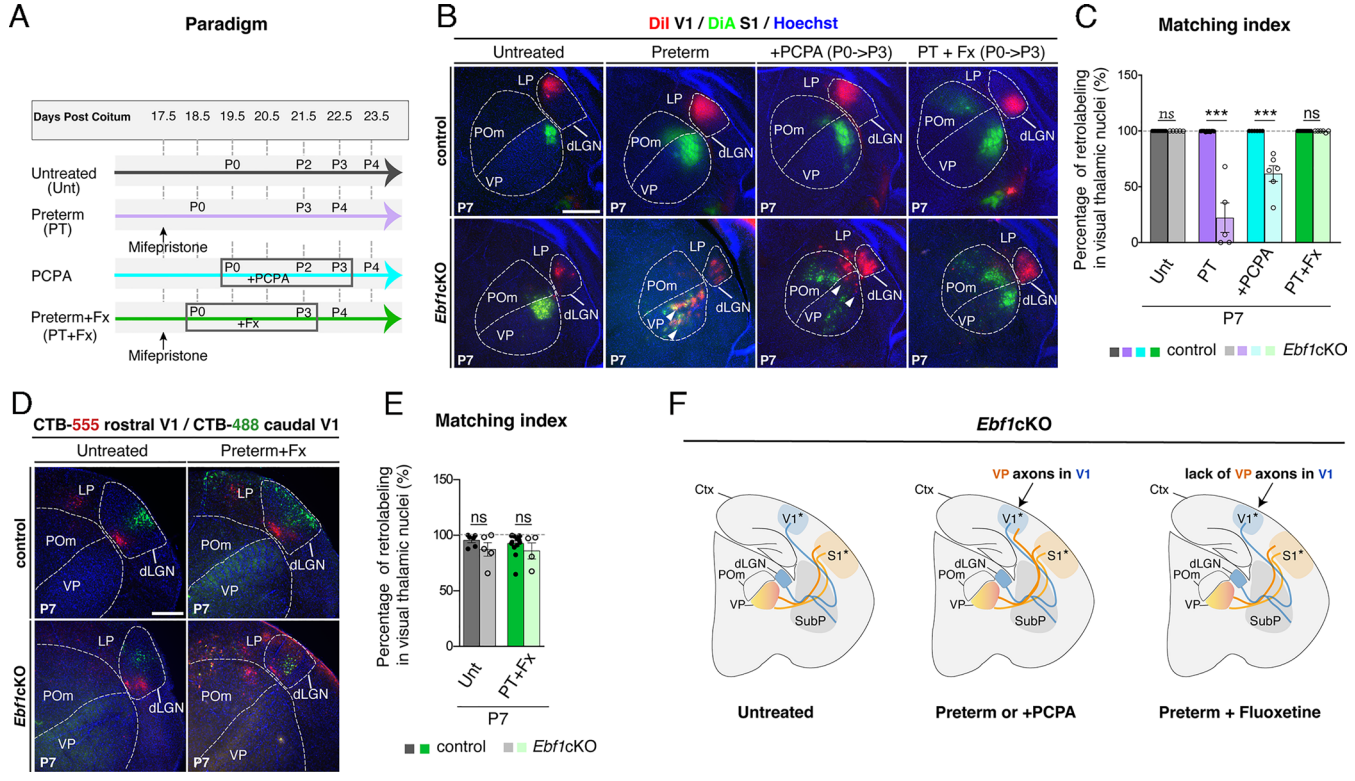

Fig. 3. Preterm birth impairs TCA plasticity partly through serotonin levels. (*A*) Experimental procedure to induce preterm birth by mifepristone injection at E17.5 and reduced or increased 5-HT levels since birth with administration of daily injections of PCPA or Fluoxetine (Fx) respectively. (*B*) Coronal section of the thalamus after DiI injection into V1 (red) and DiA injection into caudal S1 (green) in control and *Ebf1*cKO (*Dlx5/6::Cre;Ebf1*$^{fl/-}$) mice at P7 in the untreated, preterm, PCPA, or Preterm+Fx conditions. In preterm or PCPA *Ebf1*cKO at P7, V1 injection (red) simultaneously led to retrolabeling in VP and dLGN thalamic nuclei, indicating that some TCA of the VP targeted V1 instead of S1 (arrowheads). Increased 5-HT levels induced by Fx injections in preterm *Ebf1*cKO restored TCA plasticity. (*C*) Quantification of the matching index by measuring the proportion of the red signal in visual thalamic nuclei (dLGN and LP) at P7 following DiI injection into V1. Untreated$_{control}$ = 99.99 ± 0.01% (n = 9) vs. Untreated$_{mutant}$ = 99.97 ± 0.02% (n = 5); Preterm$_{control}$ = 99.73 ± 0.11% (n = 12) vs. Preterm$_{mutant}$ = 22.32 ± 13.23% (n = 5); PCPA$_{control}$ = 100 ± 0.01% (n = 6) vs. PCPA$_{mutant}$ = 61.78 ± 7.03% (n = 5); Preterm+Fx$_{control}$ = 100 ± 0.01% (n = 10) vs. Preterm+Fx$_{mutant}$ = 99.72 ± 0.27% (n = 6). (*D*) Coronal section of the thalamus after CTB-555 injection into rostral V1 (red) and CTB-488 injection into caudal V1 (green) in control and *Ebf1*cKO mice at P7 in the untreated and Preterm+Fx conditions, demonstrating that increased 5-HT levels in preterm *Ebf1*cKO induced by Fx injections restore TCA plasticity. (*E*) Quantification of the matching index by measuring the proportion of the signal in visual thalamic nuclei (dLGN and LP) at P7 following the injections of CTB into V1. Untreated$_{control}$ = 95.51 ± 2.18% (n = 6) vs. Untreated$_{mutant}$ = 87.22 ± 6.12% (n = 5); Preterm+Fx$_{control}$ = 92.67 ± 2.52% (n = 14) vs. Preterm+Fx$_{mutant}$ = 85.92 ± 7.25% (n = 14). (*F*) Decreased 5-HT levels induced by PCPA injections since birth mimicked the defect of TCA plasticity observed in preterm *Ebf1*cKO at P7. Conversely, increased 5-HT levels induced by Fx injections in preterm *Ebf1*cKO restored TCA plasticity. Values are presented as mean ±SEM; ***P < 0.001, two-way ANOVA with Sidak's correction for multiple comparisons (Scale bars, 250 µm). Ctx, cortex; dLGN, dorsal lateral geniculate nucleus; LP, lateral posterior nucleus; POm, posteromedial nucleus; S1, primary somatosensory cortex; SubP, subpallium; V1, primary visual cortex; VP, ventroposterior nucleus. See also *SI Appendix*, Figs. S5, S6, and S8.

was sufficient to fully rescue the plasticity defect and led to a similar pattern of TCA wiring as seen in untreated conditions (Fig. 3 *B* and *C*). Remarkably, double CTB injections into V1 (*SI Appendix*, Fig. S5*A*) confirmed that Fx exposure from birth was sufficient to fully rescue TCA plasticity in PT *Ebf1*cKO conditions since no retrolabeled VP neurons were detected (Fig. 3 *D* and *E*). Importantly, this rescue was not due to increased elimination of mistargeted TCA, as increasing 5-HT levels by Fx injections in the PT condition promoted cell survival in both controls and mutants (*SI Appendix*, Fig. S6). Altogether, these results demonstrate that the postnatal window of TCA plasticity is dependent on 5-HT levels and modulated by birth. Indeed, while preterm birth or pharmacological decrease in 5-HT levels impairs TCA plasticity in mutants, revealed by mistargeted VP axons in V1, increasing 5-HT levels after preterm birth rescues axonal plasticity and restores matching with their target cortical areas (Fig. 3*F*).

Efficient Plasticity Is Required for Primary Area Border Integrity. It has been well documented that thalamic inputs are required to establish the identity of cortical areas identity (29, 30, 47–49, 65). Given that preterm birth or reduction of 5-HT levels from birth (Figs. 2 and 3) lead to abnormal maintenance of VP axons in V1, we examined its impact on cortical arealization, particularly on the V1 identity and border formation. We first performed in situ hybridization for cortical markers *Rorβ* and *Lmo4* on flattened control and mutant cortices in the untreated, PT, PCPA, and PT+Fx conditions at P7 (Fig. 4*A*). Considering the reduction in the size of primary areas and a concomitant increase in the PTLp width in untreated *Ebf1*cKO (Fig. 1), we confirmed that none of the conditions affected the areal representation neither in control nor in mutant (*SI Appendix*, Fig. S7).

Using in situ hybridization for cortical markers (Fig. 4*A*), we observed that in *Ebf1c*KO PT, in which some VP axons persisted in V1, the molecular identity of the V1 border was altered compared to control, where blurred expression of *Rorβ* and *Lmo4* prevented clear delineation of the border (Fig. 4*A*). To quantify the deficits in boundaries sharpness, we calculated the average gradient (∇) of the cortical marker expression, *Rorβ* and *Lmo4,* at the V1-PTLp border. We observed a significant defect in *Ebf1c*KO PT compared to the untreated control or untreated mutant conditions (Fig. 4*B*). Furthermore, in the PCPA *Ebf1c*KO condition, which decrease 5-HT levels and partly recapitulates the TCA plasticity defect seen in PT *Ebf1*cKO, a similar defect in molecular markers of border identity was observed (Fig. 4 *A* and *B*). Finally, in the PT+Fx mutant condition, where TCA plasticity was rescued through increased 5-HT levels, we saw a complete restoration of the sharp V1 border gradient (Fig. 4 *A* and *B*).

Overall, our study demonstrates that PT birth affects early postnatal capacity of TCA to rewire after embryonic mistargeting and prevents the successful matching of somatosensory–VP axons to S1 in *Ebf1*cKO. This persistent mismatch affects the molecular identity and formation of a well-defined V1 border; however, this defect can be restored by increasing 5-HT levels in PT mutants from birth, which highlights the impact of preterm birth and serotonin-sensitive early postnatal period on the plasticity of a major axonal projection of the brain.

Discussion

Mammalian sensory perception relies on the transfer of peripheral inputs conveyed via the thalamus to appropriate cortical areas and the formation of functional maps (9, 11). Elucidating the mechanisms underlying the wiring of distinct sensory TCA connections is thus critical for the understanding of area sensory circuits and their functioning. Here, we showed that embryonic TCA mistargeting could be efficiently corrected during a short postnatal period through sequential developmental events that enable plastic adaptation of sensory modalities. Furthermore, we revealed that this short window of plasticity following birth, during which TCA get readdressed to their proper cortical target areas, is sensitive to the timing of birth and 5-HT levels. We also demonstrated that this remarkable plastic feature of TCA is critical for the formation of molecularly well-defined cortical areas.

The postnatal ability of TCA to correct developmental defects has been previously reported in studies using various mouse models (16, 47, 51, 52, 66, 67). Nevertheless, the exact timing of the sequential events underlying this ability has not yet been fully described. Here, we leveraged the *Ebf1*cKO mouse model (14), characterized by defective embryonic TCA pathfinding induced by an abnormal development of intermediate targets. In this model, defective TCA pathfinding leads to abnormal innervation at birth: somatosensory–VP axons target V1 instead of S1, while visual-dLGN axons do not yet innervate the cortex. We found that this misguidance induces a massive embryonic apoptosis of thalamic neurons, specifically in primary thalamic nuclei (VP and dLGN), which precedes postnatal cross-areal rewiring of TCA (16, 20, 68, 69). While the exact role of this embryonic cell death in axonal plasticity remains largely unknown, we observed, as expected, a subsequent reduction in the size of apoptotic primary thalamic nuclei (VP and dLGN) as well as their corresponding representation in the sensory cortices (S1 and V1) (47, 48, 67). Nevertheless, these reduced areas were molecularly well defined and responsive to specific sensory modalities, which supports the remarkable adaptive capacity of the sensory system to reshape and match thalamic inputs with their corresponding primary cortical areas.

By taking advantage of *Ebf1*cKO, we highlighted that a relatively short time window supports TCA rewiring following birth, and it depends on levels of 5-HT. In mammals, delivery is a complex biological phenomenon that triggers several environmental and hormonal changes (70), including a decrease in 5-HT (38). Therefore, we investigated whether accelerated birth or reducing levels of 5-HT modulate the process of TCA rewiring. We found that inducing preterm birth (38, 61) perturbs axonal rewiring in *Ebf1*cKO, causing a persistence of some VP axons to abnormally innervate V1 in concert with dLGN axons. Precipitating a decrease in 5-HT during the window of plasticity [PCPA injections from P0 to P3; (38, 41)] mimicked the effects of the preterm condition, where enduring mistargeted VP axons were observed in V1. Importantly, increasing 5-HT levels in preterm *Ebf1*cKO pups by Fx injections (71) was sufficient to fully restore cross-areal plasticity of TCA, supporting the fact that 5-HT modulates axonal rewiring. It is known that a postnatal decrease in 5-HT is critical for TCA development (38, 39, 72): Excess in 5-HT prevents TCA clustering and sensory map formation (40, 42, 46, 73), whereas 5-HT absence, in contrast, has no apparent impact on these processes (72, 74, 75). Here, we defined a 5-HT-dependent time window and demonstrated the importance of maintaining 5-HT levels shortly after birth to enable the efficient rescue of TCA wiring in the context of embryonic mistargeting. However, a subsequent decrease allows the formation of sensory maps (40, 42, 46, 73) and cortical circuits (45). Further experiments are needed to determine whether 5-HT acts upon this plasticity window via an indirect process or by acting directly on growing axons (38, 40, 42, 76) potentially by modulating their response to guidance cues as previously proposed (72, 77, 78). Irrespective of the underlying mechanisms, our study revealed that preterm birth and decrease in 5-HT levels in mice impair the postnatal time window of TCA plasticity and adaptation.

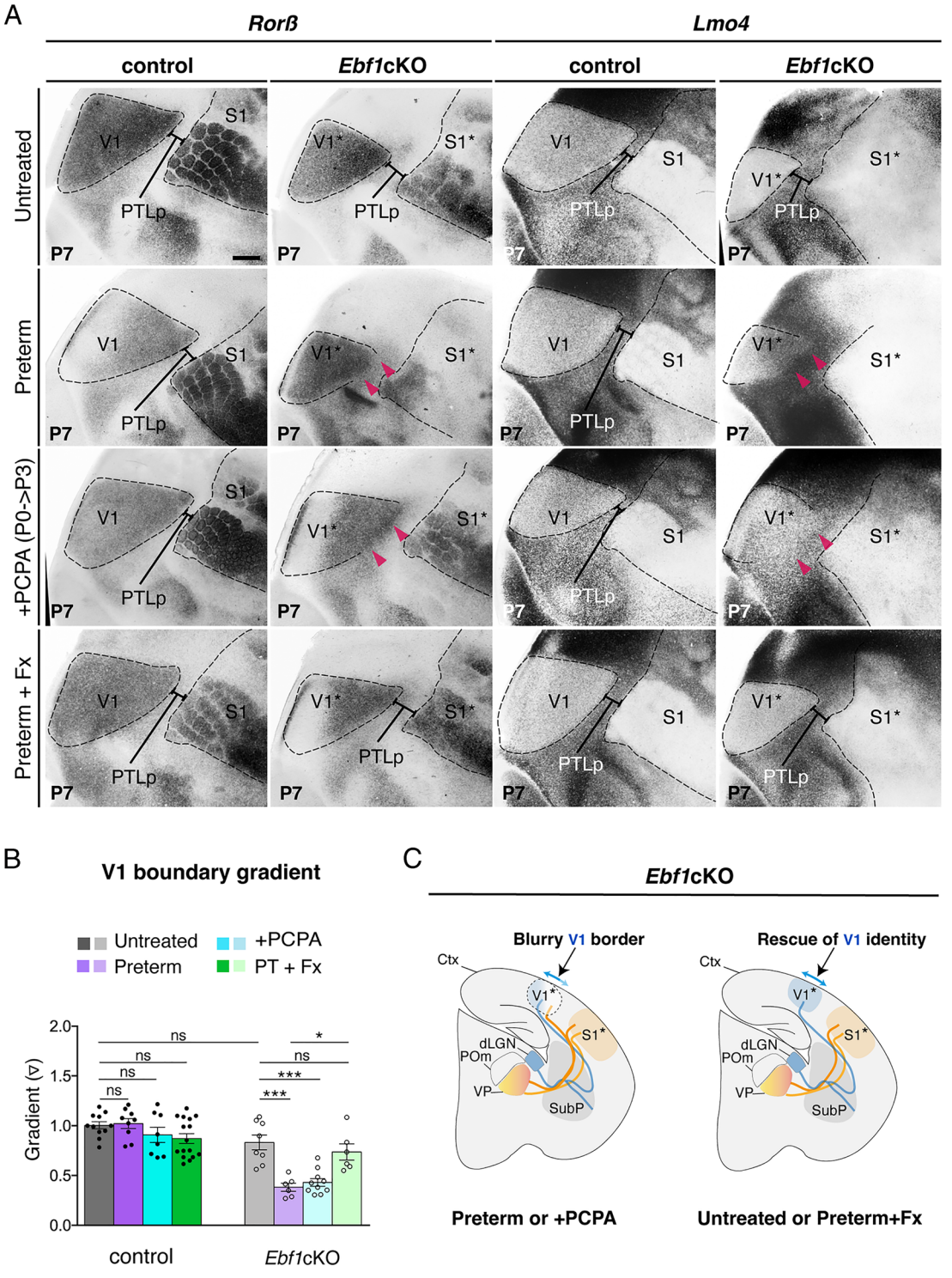

Fig. 4. TCA plasticity impairment impacts molecular identity of the V1 border. (*A*) In situ hybridization flattened cortex at P7 using specific cortical markers *Rorβ* and *Lmo4* in control and *Ebf1*cKO (*Dlx5/6::Cre;Ebf1*$^{fl/-}$) mice in the untreated ($n_{control}$ = 11; n_{mutant} = 8), preterm ($n_{control}$ = 9; n_{mutant} = 6), PCPA ($n_{control}$ = 8; n_{mutant} = 10) or Preterm+Fx ($n_{control}$ = 16; n_{mutant} = 6) conditions. In the preterm and PCPA *Ebf1*cKO conditions, the molecular identity of the V1 border was affected, according to the blurry expression of *Rorβ* and *Lmo4* (pink arrowheads) compared to its sharp delineation in controls or untreated *Ebf1*cKO. Fx injections in the preterm *Ebf1*cKO condition restored the well-defined molecular identity. (*B*) Quantification of the V1 boundary gradient observed with in situ hybridization. $Control_{Untreated}$ = 1.005 ± 0.037 (n = 11) vs. $Control_{Preterm}$ = 1.023 ± 0.05 (n = 9) vs. $Control_{PCPA}$ = 0.909 ± 0.08 (n = 8) vs. $Control_{Preterm+Fx}$ = 0.870 ± 0.07 (n = 16) and $Mutant_{Untreated}$ = 0.833 ± 0.07 (n = 8) vs. $Mutant_{Preterm}$ = 0.38 ± 0.04 (n = 6) vs. $Mutant_{PCPA}$ = 0.43 ± 0.03 (n = 10) vs. $Mutant_{Preterm+Fx}$ = 0.74 ± 0.08 (n = 6). (*C*) Defective V1 molecular identity in the preterm and PCPA *Ebf1*cKO conditions while Fx injections in preterm *Ebf1*cKO rescued the sharpness of the V1 border at a level comparable to that in the untreated control condition. Values are presented as mean ± SEM; *P < 0.05, ***P < 0.001, two-way ANOVA with Sidak's correction for multiple comparisons (Scale bars, 250 μm)=; Ctx, cortex; dLGN, dorsal lateral geniculate nucleus; LP, lateral posterior nucleus; POm, posteromedial nucleus; PTLp, posterior parietal association area; S1, primary somatosensory cortex; SubP, subpallium; V1, primary visual cortex; VP, ventroposterior nucleus. See also *SI Appendix*, Fig. S7.

Compared to mice, embryogenesis in humans is protracted, and the first postnatal week in mice roughly corresponds to the third trimester of gestation in human fetuses (3, 79). If conserved, the time window of TCA plasticity identified here could be present in humans at the beginning of the third trimester, specifically, when TCA start to target cortical sensory areas (3, 79, 80). Preterm

birth across this period in humans (corresponding to human very preterm birth) has been associated with modifications in sensory areas size (81), thalamic volume and connectivity (3, 6, 82–85), and cognitive impairment and linked with neurodevelopmental disorders, including autism spectrum disorders and schizophrenia (6–8, 86). Thus, the developmental time window identified in our study might be relevant to deficits associated with very preterm birth in humans, potentially preventing the proper rescue of prenatal deficits that would normally be corrected by plastic adaptation.

The long-term consequences of mistargeted TCA remain to be explored, particularly whether they activate inappropriate modalities, which would lead to cross-modal activation following somatosensory stimulation (87, 88). Yet, our study showed that TCA mistargeting triggers defects in cortical arealization, particularly for the V1 border and the interposed HO PTLp. Interestingly, dysfunction in human PTLp has been linked with clinical deficits since this area integrates all sensory modalities and appears notably crucial for multiple cognitive processes, which include sensorimotor integration, spatial navigation, or decision-making (54, 55, 84, 89).

In conclusion, our findings reveal that a short postnatal birth- and 5-HT-dependent plastic window identified in our genetic mouse model contributes to restoring embryonic TCA axon misguidance. The findings open the intriguing possibility that impairments during this plasticity window may have pathological consequences contributing to the complex physiology associated with neurodevelopmental disorders.

Materials and Methods

Mouse Lines. *Dlx5/6::Cre;Ebf1*$^{fl/-}$ mutant animals were obtained by crossing *Dlx5/6::Cre* mice with *Ebf1*$^{+/-}$ mice to generate *Dlx5/6::Cre;Ebf1* offspring. *Dlx5/6::Cre;Ebf1*$^{+/-}$ mice were then crossed with *Ebf1*$^{fl/fl}$ animals to produce *Dlx5/6::Cre;Ebf1*$^{fl/-}$ conditional knockout mice (14). All these lines were maintained on a C57/Bl6J genetic background. The TCA-GFP Tg line was kindly provided by Pr. Takuji Iwasato (56) and backcrossed in *Ebf1*$^{fl/fl}$ background. Embryonic day (E) 0.5 was designated as the day of vaginal plug detection, while postnatal day (P) 0 was designated as the day of birth. Animals were handled in accordance with the European Union regulations and the rules of the local ethics committee.

Pharmacological and Surgical Manipulations.

Mifepristone treatment. Mifepristone treatment was carried out as described elsewhere with modifications (38). Mifepristone (Calbiochem, San Diego, CA, USA) was dissolved at 10 mg/mL in ethanol and stored at −20 °C. Then, pregnant female mice were given subcutaneous injections of 150 μL of 1 mg/mL mifepristone solution diluted in saline at E17.5 between 17:30 and 18:30. Mouse pups were born between 12:00 and 18:00 the following day.

PCPA treatment. PCPA treatment was performed as described elsewhere (38). PCPA (Sigma, St. Louis, MO, USA) was dissolved in saline at 10 mg/mL. Pups were given subcutaneous PCPA injections at 300 mg/kg daily from P0 to P3 until they were euthanized.

Fx treatment on preterm. Fx (Tocris, Bristol, UK) was dissolved in 0.9% NaCl solution at 0.5 mg/mL. Pregnant mice, followed by pups, were given subcutaneous injections of 10 mg/kg Fx at E17.5 and then from P0 to P3 until they were killed.

ION sectioning. ION sectioning was performed on P0 pups. Animals were cryoanesthetized on ice. The right ION was sectioned as previously described by ref. 90. Pups were brought out of cryoanesthesia on a heating pad and then returned to the mother until they were killed.

In Situ Hybridization and Immunohistochemistry. For in situ hybridization, pups were perfused with 4% paraformaldehyde (PFA) in phosphate-buffered solution (PBS), dissected, flattened, and postfixed in 4% PFA overnight at 4 °C. For flattening, intact cortices were isolated from subcortical tissue by dissection, sandwiched between two Superfrost microscope slides separated by 1-mm spacers and postfixed in 4% PFA overnight at 4 °C. The following day, fixed flattened cortices were cut into 120-μm free-floating sections using a Leica S1000 vibratome and hybridized with digoxigenin-labeled probes *Cadherin 8, Cadherin 6, Lhx9, Igfbp5, Lmo4,* and *Rorβ* as described elsewhere (91).

For immunohistochemistry, whole brains or flattened cortices were cut into 70-μm free-floating sections using a Leica S1000 vibratome. Slices were incubated in a blocking solution containing 0.25% Triton X-100 (Sigma, St. Louis, MO, USA) and 0.02% gelatin in PBS for 1 h at room temperature and incubated in the same blocking solution with primary antibodies overnight at 4 °C. Primary antibodies were used at the following concentrations: Rabbit anti-Calretinin 1/1,000 (Calb2, 7697, Swant, Burgdorf, Switzerland), Rabbit anti-Caspase-3 cleaved 1/400 (AF835; R&D systems, Minneapolis, MN, USA), Goat anti-Foxp2 1/200 (21069; Santa Cruz, Heidelberg, Germany), Chicken anti-GFP 1/1,000 (GFP-1020; Avès, Davis, CA, USA), Goat anti-NetrinG1a 1/100 (AF1166; R&D systems, Minneapolis, MN, USA), Rabbit anti-5-HTT 1/1,000 (PC177L; Calbiochem, San Diego, CA, USA) and Guinea pig anti-vGLUT2 1/1,000 (AB2251; Millipore, Burlington, MA, USA). The next day, the sections were rinsed four times in PBS and incubated with the corresponding secondary antibodies in PBS overnight at 4 °C. Secondary antibodies were used at 1/400 and included A488-conjugated donkey anti-rabbit and chicken, Cy3-conjugated donkey anti-rat and anti-goat, and DyLight488-conjugated donkey anti-guinea pig (Jackson ImmunoResearch, Baltimore, PA, USA). Hoechst (Sigma, St. Louis, MO, USA) was used for fluorescent nuclear counterstaining, and sections were mounted in Vectashield (Vector, Newark, CA, USA).

Axonal Tracing: Carbocyanine Dye and CTB injections. For axonal tracing using dyes, embryonic and perfused postnatal brains were fixed in 4% PFA at least overnight at 4 °C. Crystals of DiI (1,1′-dioctadecyl 3,3,3′,3′-tetramethylin docarbo-cyanine perchlorate; Invitrogen, USA) or DiA [4-(4-(dihexadecylamino) styryl)-N-methylpyridinium iodide; Invitrogen, USA] were inserted into either the thalamus or neocortex of intact hemisected brains. Injected brains were incubated at 37 °C, and dye diffusion was assessed every week by whole-brain examination under a fluorescent binocular set-up (Leica MZ16 F).

For axonal tracing using CTB, P4 pups were cryoanesthetized on the ice during 1′30″. Then, 200 nL of each Alexa Fluor 488 (C34775) and Alexa Fluor 555 (C34776) Conjugated Cholera Toxin Subunit B (Invitrogen, USA) were both injected into respectively the caudal and rostral V1 areas at 1 μg/μL. Pups were brought out of cryoanesthesia on a heating pad and then returned to the mother until P8, when brains were perfused and fixed in 4% PFA at least overnight at 4 °C.

Pictures of representative cortical injection sites on hemi-brains were acquired using a Leica MZ16F Binocular at different developmental stages and conditions (*SI Appendix*, Fig. S8). Brains were then cut into 100 μm-thick free-floating sections using a Leica S1000 vibratome, and the sections were counterstained using Hoechst (Sigma, St. Louis, MO, USA). Staining was visualized under a fluorescent Leica DM5000 B or DMI8 microscope and examined at the level of the internal capsule and/or thalamus.

Image Acquisition and Quantifications. Images were acquired using a fluorescence binocular microscope (Leica MZ16F), a fluorescence microscope (Leica DM5000 B & Leica DMI8), and a confocal microscope (Leica TCS SP5). Image analyses were performed with ImageJ (NIH) and Adobe Photoshop software.

Thalamic nuclei size quantification. Thalamic structures, including dLGN, LP, VP, and POm were identified on coronal sections of the mouse brain using immunolabeling (FoxP2, Calb2, vGlut2, or NetG1) or Hoechst delineation. As the VP size is severely reduced in *Ebf1*cKO, to properly compare the equivalent rostrocaudal level, we chose the barreloid level in mutants, which is represented in one 70μm-thick section and compared with matching rostrocaudal levels in controls. The size of each thalamic nucleus was extracted in each sample using ImageJ software, and the percentage (%) of the mutant size compared to the control was calculated.

Apoptosis quantification. dLGN, LP, POm, and VP thalamic structures were identified on immunolabeled coronal sections of mouse brain using anti-vGlut2 (*In Situ Hybridization and Immunohistochemistry*) and Hoechst (Sigma, St. Louis, MO, USA) signal. The level of the apoptotic anti-cCasp3 (*In Situ Hybridization and Immunohistochemistry*) signal within each thalamic structure was quantified on two or three rostrocaudal levels for each brain as follows: The anti-cCasp3 signal was thresholded using the automated Threshold function in ImageJ, and the signal coverage (%) was subsequently calculated for each demarcated thalamic structure.

Area size and localization quantification. PTLp, S1, and V1 areal structures were identified on tangential sections of the flattened cortex using anti-vGlut2 signal domains (see *In Situ Hybridization and Immunohistochemistry*) from immunolabeling experiments and *Cadherin 8, Igfbp5, Lmo4,* and *Rorβ* signal from in situ hybridization experiments. The size of an individual areal structure visualized using a specific marker was calculated as the percentage (%) of the average size of the same structure visualized using the same marker in littermate controls.

To assess the localization of S1 and V1 in mutant vs. control, TCA-GFP fluorescence observed in whole brains was examined (using a Leica fluorescent binocular MZ16F), which allowed the easy visualization of primary areas within the neocortex. As presented in *SI Appendix*, Fig. S3*B*, the localization of V1 and S1 boundaries was determined by measuring the distance of the middle of V1 from the caudal midline (mD) and the distance of S1 from the middle of V1 (cD) as well as the distance of S1 from the midline (mD).

Matching index quantification using carbocyanine dye and CTB axonal tracing. dLGN/LP and VP/POm thalamic structures were identified on coronal sections of the mouse brains, following DiI or CTB injections into V1 and using Hoechst (Sigma, St. Louis, MO, USA) signal. While DiI is a nonspecific retrograde marker, CTB is commonly used as a retrograde tracer to label TCA (62). Overall, the DiI/DiA approach allowed us to selectively label dLGN TCA during early postnatal stages, as reciprocal corticothalamic axons were not yet innervating dLGN (92), which was appreciated by retrolabeling of neuronal cell bodies in the thalamus. The level of fluorescent signal inside the dLGN/LP and VP/POm thalamic structures was quantified, the fluorescent signal was thresholded using the automated Threshold function in ImageJ, and the area of signal (px) was calculated separately for the dLGN/LP and VP/POm. These quantifications were used to calculate the percentage of signal detected in the visual dLGN/LP over the signal detected in both visual dLGN/LP and somatosensory-VP/POm. To compensate for the variability in thalamic retrolabeling between different injected brains, we calculated and compared the matching index, defined as the percentage of fluorescent signal in dLGN/LP vs. the dLGN/LP+VP/POm combined, with 100% representing fluorescent signal distributed exclusively in the dLGN/LP and absent in the VP/POm (*SI Appendix*, Fig. S3*D*).

Barrel field intensity (BFI) index. Maturation of the barrel field across time was defined by the BFI index measured according to ref. 38. We used GFP-stained tangential sections of the *TCA-GFP* flattened cortex in normal and preterm birth conditions at different postnatal stages (P2 to P4). Optical densities were measured along the line of caudal barrels (between C1 and C3) using ImageJ. The BFI was calculated as the contrast between the intensity of C2 and the average intensity of adjacent spaces separating C2 from C1 and C3, normalized by the average intensity of the whole barrel region. Thus, BFI values increased when TCA axons started to enhance clustering to innervate the barrels.

V1-PTLp boundary quantification. The V1-PTLp boundary region was identified on tangential sections of the flattened cortex using either the *Lmo4* or *Rorβ* signal from in situ hybridization experiments. We obtained ImageJ Plot Profiles of the signal intensity a length of 100 px set perpendicular to V1-PTLp boundary and centered on it. For each specimen, the Plot Profile measurements were acquired over three nonoverlapping regions of the V1-PTLp boundary. The slot of intensity signal with a width of 20 px around the V1-PTLp boundary, as well as the sharpness of the boundary, was determined by calculating the average gradient (∇) corresponding to the mean of values. A steeper gradient corresponded to a clearer demarcation of the V1-PTLP boundary and vice versa.

Voltage-Sensitive Dye (VSD) Imaging. VSD imaging of the cortical activity evoked by visual and tactile whiskers stimulation was performed on adult mice under isoflurane anesthesia (induction: 3 to 4%, maintenance: 1 to 1.5%), as described elsewhere (59, 60). Briefly, the left barrel cortex was exposed and stained for 1 h with the VSD RH1691 (1 mg/mL, in Ringer's solution containing [in mM]: 135 NaCl, 5 KCl, 5 HEPES, 1.8 CaCl2, and 1 MgCl2). After removal of the unbound dye, the cortex was covered with agarose (0.5 to 1% in Ringer's) and a coverslip. Cortical imaging was performed using a tandem-lens fluorescence microscope (SciMedia, Costa Mesa, CA, USA), equipped with one Leica PlanApo 1.6× (objective side) and one Leica PlanApo 0.63× (condensing side), a 630-nm excitation filter, a 650-nm dichroic mirror, and a long-pass 665-nm emission filter. The resulting field of view was 3.8 × 3.8 mm, with a pixel resolution of 38 × 38 μm. Visual stimulation was performed using a single brief flash (50 or 100 ms) of a green light-emitting diode placed at about 5 cm in front of the animal's binocular field of view. Tactile stimulation of the whiskers consisted of one brief rostral deflection (2-ms rising time, 2-ms plateau, and 2-ms fall) of either the alpha or C2 whisker on the right side of the snout by means of a multiwhisker stimulator (93). The whiskers were inserted, with their natural angle maintained into 27G stainless steel tubes attached to the piezoelectric benders (Noliac, Denmark), leaving 2 mm between the tip of the tube and the whisker base. Each whisker deflection consisted of a 95-μm displacement (measured at the tip of the tube). Specific filters were applied to the voltage commands to prevent mechanical ringing of the stimulators. Visual and tactile alpha and C2 whisker stimulations were delivered within pseudorandomized sequences containing extra blank trials (each stimulation being repeated 40 times). The illumination of the cortical surface started 500 ms before each image acquisition to avoid acquiring signal in the steeper phase of the fluorescence bleaching. Recordings were then of 1,000 ms duration, with 200 ms of baseline and 800 ms of poststimulation. Variations of the fluorescence signals were initially recorded as variations over the resting light intensity (first acquired frame).

Data preprocessing was performed using in-house software (Elphy, G. Sadoc, UNIC-CNRS), and further analyses were completed using custom-written routines in IgorPro (Wavemetrics). Subtraction of a pixel-by-pixel best-fit double exponential from the averaged unstimulated sequence was used to correct for photobleaching. Further subtraction of the averaged signal over three frames just preceding the stimulus was made to focus on sensory-evoked activity.

Statistical Analysis. All data are presented as mean ± SEM, and $P < 0.05$ was considered statistically significant. According to the data structure, we systematically performed nonparametric tests, namely the Mann–Whitney *U* test, and two-way ANOVA with Sidak's correction for multiple comparisons, depending on whether a single or multiple group comparison with individual or common controls was performed. Statistics and plotting were performed using GraphPad Prism 7.00 (GraphPad Software Inc., USA). $*P < 0.05$, $**P < 0.01$, $***P < 0.001$.

Data, Materials, and Software Availability. All study data are included in the article and/or *SI Appendix*.

ACKNOWLEDGMENTS. We are grateful to the members of the Garel laboratory and Dr. Evelyne Bloch-Gallego for facilitating discussions and providing critical comments on the manuscript. We thank Feriel Zehani, Déborah Souchet, Amandine Delecourt, Eléonore Touzalin, Gwendoline Firmin, Dolores Valera, and Carmen Le Moal for excellent technical support and assistance with mouse colonies. We thank Pr. Takuji Iwasato and Pr. Rudolf Grosschedl for providing respectively the TCA-GFP and *Ebf1*$^{flox/flox}$ lines for experiments. We are grateful to Dr. Clément Léna, Dr. Rémi Proville, and Dr. Maria Spolidoro for their precious insight into the project and to Master students, Simon Daste and Thandi Phillipe for their help during their internship. We thank Ilya Demchenko of Insight Editing London for the scientific editing of the manuscript. We thank the IBENS Imaging Facility (France BioImaging, supported by ANR-10-INBS-04, ANR-10-LABX-54 MEMO LIFE, and ANR-11-IDEX-000-02 PSL Research University, "Investments for the future"). The Garel laboratory is supported by INSERM, CNRS, ERC Consolidator NImO 616080, ANR-15-CE16-0003, ANR-19-CE16-0017-02, and Fonds St Michel/Fondation du Collège de France. A.L. is a recipient of a fellowship from the École des Neurosciences de Paris Île-de-France network and holds an ATER position at the Collège de France. S.G. is part of the École des Neurosciences de Paris Ile-de-France network. L.L. is an INSERM investigator.

Author affiliations: [a]Team Brain Development and Plasticity, Institut de Biologie de l'ENS, École Normale Supérieure, CNRS, INSERM, PSL Research University, 75005 Paris, France; [b]Université Paris-Saclay, CNRS, Institut des Neurosciences Paris-Saclay, 91400 Saclay, France; [c]Acute Transgenesis Facility, Institut de Biologie de l'ENS, École Normale Supérieure, CNRS, INSERM, PSL Research University, 75005 Paris, France; and [d]Collège de France, PSL Research University, 75005 Paris, France

1. C. R. Cadwell, A. Bhaduri, M. A. Mostajo-Radji, M. G. Keefe, T. J. Nowakowski, Development and arealization of the cerebral cortex. *Neuron* **103**, 980–1004 (2019).
2. I. Genescu, S. Garel, Being superficial: A developmental viewpoint on cortical layer 1 wiring. *Curr. Opin. Neurobiol.* **66**, 125–134 (2021).
3. Z. Molnar, H. J. Luhmann, P. O. Kanold, Transient cortical circuits match spontaneous and sensory-driven activity during development. *Science* **370**, eabb2153 (2020).
4. R. Cossart, S. Garel, Step by step: Cells with multiple functions in cortical circuit assembly. *Nat. Rev. Neurosci.* **23**, 395–410 (2022).

5. G. Lopez-Bendito, M. Anibal-Martinez, F. J. Martini, Cross-modal plasticity in brains deprived of visual input before vision. *Annu. Rev. Neurosci.* **45**, 471–489 (2022).
6. R. G. Brenner, M. D. Wheelock, J. J. Neil, C. D. Smyser, Structural and functional connectivity in premature neonates. *Semin. Perinatol.* **45**, 151473 (2021).
7. S. Johnson, N. Marlow, Preterm birth and childhood psychiatric disorders. *Pediatr. Res.* **69**, 11R–18R (2011).
8. M. K. Mwaniki, M. Atieno, J. E. Lawn, C. R. Newton, Long-term neurodevelopmental outcomes after intrauterine and neonatal insults: A systematic review. *Lancet* **379**, 445–452 (2012).
9. E. G. Jones, Thalamic circuitry and thalamocortical synchrony. *Philos. Trans. R. Soc. Lond. B Biol. Sci.* **357**, 1659–1673 (2002).
10. I. Vitali, D. Jabaudon, Synaptic biology of barrel cortex circuit assembly. *Semin. Cell Dev. Biol.* **35**, 156–164 (2014).
11. V. S. Caviness Jr., D. O. Frost, Tangential organization of thalamic projections to the neocortex in the mouse. *J. Comp. Neurol.* **194**, 335–367 (1980).
12. D. Jabaudon, Fate and freedom in developing neocortical circuits. *Nat. Commun.* **8**, 16042 (2017).
13. Y. Nakagawa, Development of the thalamus: From early patterning to regulation of cortical functions. *Wiley Interdiscip. Rev. Dev. Biol.* **8**, e345 (2019).
14. L. Lokmane *et al.*, Sensory map transfer to the neocortex relies on pretarget ordering of thalamic axons. *Curr. Biol.* **23**, 810–816 (2013).
15. F. Bielle *et al.*, Slit2 activity in the migration of guidepost neurons shapes thalamic projections during development and evolution. *Neuron* **69**, 1085–1098 (2011).
16. L. Lokmane, S. Garel, Map transfer from the thalamus to the neocortex: Inputs from the barrel field. *Semin. Cell Dev. Biol.* **35**, 147–155 (2014).
17. I. Dupin, L. Lokmane, M. Dahan, S. Garel, V. Studer, Subrepellent doses of Slit1 promote Netrin-1 chemotactic responses in subsets of axons. *Neural. Dev.* **10**, 5 (2015).
18. S. Backer *et al.*, Trio GEF mediates RhoA activation downstream of Slit2 and coordinates telencephalic wiring. *Development* **145**, dev153692 (2018).
19. R. S. Erzurumlu, P. Gaspar, Development and critical period plasticity of the barrel cortex. *Eur. J. Neurosci.* **35**, 1540–1553 (2012).
20. Z. Molnar, S. Garel, G. Lopez-Bendito, P. Maness, D. J. Price, Mechanisms controlling the guidance of thalamocortical axons through the embryonic forebrain. *Eur. J. Neurosci.* **35**, 1573–1585 (2012).
21. G. Lopez-Bendito, Development of the thalamocortical interactions: Past, present and future. *Neuroscience* **385**, 67–74 (2018).
22. J. G. Cunningham, J. D. Scripter, S. A. Nti, E. S. Tucker, Early construction of the thalamocortical axon pathway requires c-Jun N-terminal kinase signaling within the ventral forebrain. *Dev. Dyn.* **251**, 459–480 (2022).
23. S. Pal *et al.*, An early cortical progenitor-specific mechanism regulates thalamocortical innervation. *J. Neurosci.* **41**, 6822–6835 (2021).
24. H. Van der Loos, T. A. Woolsey, Somatosensory cortex: Structural alterations following early injury to sense organs. *Science* **179**, 395–398 (1973).
25. F. J. Martini, V. Moreno-Juan, A. Filipchuk, M. Valdeolmillos, G. Lopez-Bendito, Impact of thalamocortical input on barrel cortex development. *Neuroscience* **368**, 246–255 (2018).
26. R. S. Erzurumlu, P. Gaspar, How the barrel cortex became a working model for developmental plasticity: A historical perspective. *J. Neurosci.* **40**, 6460–6473 (2020).
27. P. Gaspar, N. Renier, Constraints on somatosensory map development: Mutants lead the way. *Curr. Opin. Neurobiol.* **53**, 43–49 (2018).
28. J. M. Wess, A. Isaiah, P. V. Watkins, P. O. Kanold, Subplate neurons are the first cortical neurons to respond to sensory stimuli. *Proc. Natl. Acad. Sci. U.S.A.* **114**, 12602–12607 (2017).
29. V. Moreno-Juan *et al.*, Prenatal thalamic waves regulate cortical area size prior to sensory processing. *Nat. Commun.* **8**, 14172 (2017).
30. N. Anton-Bolanos *et al.*, Prenatal activity from thalamic neurons governs the emergence of functional cortical maps in mice. *Science* **364**, 987–990 (2019).
31. F. J. Martini, T. Guillamon-Vivancos, V. Moreno-Juan, M. Valdeolmillos, G. Lopez-Bendito, Spontaneous activity in developing thalamic and cortical sensory networks. *Neuron* **109**, 2519–2534 (2021).
32. T. Guillamon-Vivancos *et al.*, Input-dependent segregation of visual and somatosensory circuits in the mouse superior colliculus. *Science* **377**, 845–850 (2022).
33. H. Li *et al.*, Laminar and columnar development of barrel cortex relies on thalamocortical neurotransmission. *Neuron* **79**, 970–986 (2013).
34. N. Narboux-Neme *et al.*, Neurotransmitter release at the thalamocortical synapse instructs barrel formation but not axon patterning in the somatosensory cortex. *J. Neurosci.* **32**, 6183–6196 (2012).
35. A. Matsui *et al.*, BTBD3 controls dendrite orientation toward active axons in mammalian neocortex. *Science* **342**, 1114–1118 (2013).
36. H. Sato *et al.*, Thalamocortical axons control the cytoarchitecture of neocortical layers by area-specific supply of VGF. *Elife* **11**, e67549 (2022).
37. I. Genescu *et al.*, Dynamic interplay between thalamic activity and Cajal-Retzius cells regulates the wiring of cortical layer 1. *Cell Rep.* **39**, 110667 (2022).
38. T. Toda *et al.*, Birth regulates the initiation of sensory map formation through serotonin signaling. *Dev. Cell* **27**, 32–46 (2013).
39. A. Teissier, M. Soiza-Reilly, P. Gaspar, Refining the role of 5-HT in postnatal development of brain circuits. *Front. Cell Neurosci.* **11**, 139 (2017).
40. A. Rebsam, I. Seif, P. Gaspar, Refinement of thalamocortical arbors and emergence of barrel domains in the primary somatosensory cortex: A study of normal and monoamine oxidase a knock-out mice. *J. Neurosci.* **22**, 8541–8552 (2002).
41. A. Rebsam, I. Seif, P. Gaspar, Dissociating barrel development and lesion-induced plasticity in the mouse somatosensory cortex. *J. Neurosci.* **25**, 706–710 (2005).
42. N. Salichon *et al.*, Excessive activation of serotonin (5-HT) 1B receptors disrupts the formation of sensory maps in monoamine oxidase a and 5-ht transporter knock-out mice. *J. Neurosci.* **21**, 884–896 (2001).
43. F. Vahid-Ansari, P. R. Albert, Rewiring of the serotonin system in major depression. *Front. Psychiatry* **12**, 802581 (2021).
44. B. Lotto, L. Upton, D. J. Price, P. Gaspar, Serotonin receptor activation enhances neurite outgrowth of thalamic neurones in rodents. *Neurosci. Lett.* **269**, 87–90 (1999).
45. F. K. Wong *et al.*, Serotonergic regulation of bipolar cell survival in the developing cerebral cortex. *Cell Rep.* **40**, 111037 (2022).
46. X. Chen *et al.*, Disruption of transient serotonin accumulation by non-serotonin-producing neurons impairs cortical map development. *Cell Rep.* **10**, 346–358 (2015).
47. G. Pouchelon *et al.*, Modality-specific thalamocortical inputs instruct the identity of postsynaptic L4 neurons. *Nature* **511**, 471–474 (2014).
48. T. Y. Vue *et al.*, Thalamic control of neocortical area formation in mice. *J. Neurosci.* **33**, 8442–8453 (2013).
49. S. J. Chou *et al.*, Geniculocortical input drives genetic distinctions between primary and higher-order visual areas. *Science* **340**, 1239–1242 (2013).
50. L. Frangeul *et al.*, A cross-modal genetic framework for the development and plasticity of sensory pathways. *Nature* **538**, 96–98 (2016).
51. G. E. Little *et al.*, Specificity and plasticity of thalamocortical connections in Sema6A mutant mice. *PLoS Biol.* **7**, e98 (2009).
52. T. Shimogori, E. A. Grove, Fibroblast growth factor 8 regulates neocortical guidance of area-specific thalamic innervation. *J. Neurosci.* **25**, 6550–6560 (2005).
53. A. Tinterri *et al.*, Active intermixing of indirect and direct neurons builds the striatal mosaic. *Nat. Commun.* **9**, 4725 (2018).
54. D. Lyamzin, A. Benucci, The mouse posterior parietal cortex: Anatomy and functions. *Neurosci. Res.* **140**, 14–22 (2019).
55. K. Hovde, M. Gianatti, M. P. Witter, J. R. Whitlock, Architecture and organization of mouse posterior parietal cortex relative to extrastriate areas. *Eur. J. Neurosci.* **49**, 1313–1329 (2019).
56. H. Mizuno *et al.*, NMDAR-regulated dynamics of layer 4 neuronal dendrites during thalamocortical reorganization in neonates. *Neuron* **82**, 365–379 (2014).
57. L. C. Greig, M. B. Woodworth, M. J. Galazo, H. Padmanabhan, J. D. Macklis, Molecular logic of neocortical projection neuron specification, development and diversity. *Nat. Rev. Neurosci.* **14**, 755–769 (2013).
58. D. Jabaudon, S. J. Shnider, D. J. Tischfield, M. J. Galazo, J. D. Macklis, RORbeta induces barrel-like neuronal clusters in the developing neocortex. *Cereb. Cortex* **22**, 996–1006 (2012).
59. I. Ferezou, S. Bolea, C. C. Petersen, Visualizing the cortical representation of whisker touch: Voltage-sensitive dye imaging in freely moving mice. *Neuron* **50**, 617–629 (2006).
60. A. Grinvald, R. Hildesheim, VSDI: A new era in functional imaging of cortical dynamics. *Nat. Rev. Neurosci.* **5**, 874–885 (2004).
61. D. J. Dudley, D. W. Branch, S. S. Edwin, M. D. Mitchell, Induction of preterm birth in mice by RU486. *Biol. Reprod.* **55**, 992–995 (1996).
62. W. L. Conte, H. Kamishina, R. L. Reep, Multiple neuroanatomical tract-tracing using fluorescent Alexa Fluor conjugates of cholera toxin subunit B in rats. *Nat. Protoc.* **4**, 1157–1166 (2009).
63. M. Soiza-Reilly *et al.*, SSRIs target prefrontal to raphe circuits during development modulating synaptic connectivity and emotional behavior. *Mol. Psychiatry* **24**, 726–745 (2019).
64. J. R. Homberg, D. Schubert, P. Gaspar, New perspectives on the neurodevelopmental effects of SSRIs. *Trends Pharmacol. Sci.* **31**, 60–65 (2010).
65. T. Monko, J. Rebertus, J. Stolley, S. R. Salton, Y. Nakagawa, Thalamocortical axons regulate neurogenesis and laminar fates in the early sensory cortex. *Proc. Natl. Acad. Sci. U.S.A.* **119**, e2201355119 (2022).
66. M. Armentano *et al.*, COUP-TFI regulates the balance of cortical patterning between frontal/motor and sensory areas. *Nat. Neurosci.* **10**, 1277–1286 (2007).
67. A. Zembrzycki, S. J. Chou, R. Ashery-Padan, A. Stoykova, D. D. O'Leary, Sensory cortex limits cortical maps and drives top-down plasticity in thalamocortical circuits. *Nat. Neurosci.* **16**, 1060–1067 (2013).
68. L. Ma *et al.*, Neurotrophin-3 is required for appropriate establishment of thalamocortical connections. *Neuron* **36**, 623–634 (2002).
69. G. Lopez-Bendito, Z. Molnar, Thalamocortical development: How are we going to get there? *Nat. Rev. Neurosci.* **4**, 276–289 (2003).
70. N. H. Hillman, S. G. Kallapur, A. H. Jobe, Physiology of transition from intrauterine to extrauterine life. *Clin. Perinatol.* **39**, 769–783 (2012).
71. M. Soiza-Reilly *et al.*, Correction: SSRIs target prefrontal to raphe circuits during development modulating synaptic connectivity and emotional behavior. *Mol. Psychiatry* **24**, 773 (2019).
72. E. S. van Kleef, P. Gaspar, A. Bonnin, Insights into the complex influence of 5-HT signaling on thalamocortical axonal system development. *Eur. J. Neurosci.* **35**, 1563–1572 (2012).
73. A. M. Persico *et al.*, Barrel pattern formation requires serotonin uptake by thalamocortical afferents, and not vesicular monoamine release. *J. Neurosci.* **21**, 6862–6873 (2001).
74. S. Trowbridge, N. Narboux-Neme, P. Gaspar, Genetic models of serotonin (5-HT) depletion: What do they tell us about the developmental role of 5-HT? *Anat. Rec. (Hoboken)* **294**, 1615–1623 (2011).
75. N. Narboux-Neme *et al.*, Postnatal growth defects in mice with constitutive depletion of central serotonin. *ACS Chem. Neurosci.* **4**, 171–181 (2013).
76. A. Bonnin, W. Peng, W. Hewlett, P. Levitt, Expression mapping of 5-HT1 serotonin receptor subtypes during fetal and early postnatal mouse forebrain development. *Neuroscience* **141**, 781–794 (2006).
77. A. Bonnin, M. Torii, L. Wang, P. Rakic, P. Levitt, Serotonin modulates the response of embryonic thalamocortical axons to netrin-1. *Nat. Neurosci.* **10**, 588–597 (2007).
78. L. Xing *et al.*, A serotonin circuit acts as an environmental sensor to mediate midline axon crossing through EphrinB2. *J. Neurosci.* **35**, 14794–14808 (2015).
79. Z. Krsnik, V. Majic, L. Vasung, H. Huang, I. Kostovic, Growth of thalamocortical fibers to the somatosensory cortex in the human fetal brain. *Front. Neurosci.* **11**, 233 (2017).
80. F. P. McCarthy, R. M. Ryan, L. C. Chappell, Prospective biomarkers in preterm preeclampsia: A review. *Pregnancy Hypertens.* **14**, 72–78 (2018).
81. E. Courchesne *et al.*, Mapping early brain development in autism. *Neuron* **56**, 399–413 (2007).
82. K. A. Cheon *et al.*, Involvement of the anterior thalamic radiation in boys with high functioning autism spectrum disorders: A Diffusion Tensor Imaging study. *Brain Res.* **1417**, 77–86 (2011).
83. Y. Jiang, M. H. Patton, S. S. Zakharenko, A case for thalamic mechanisms of Schizophrenia: Perspective from modeling 22q11.2 deletion syndrome. *Front. Neural. Circuits* **15**, 769969 (2021).
84. A. Teissier, A. Pierani, Wiring of higher-order cortical areas: Spatiotemporal development of cortical hierarchy. *Semin. Cell Dev. Biol.* **118**, 35–49 (2021).
85. W. J. Hwang *et al.*, Thalamic connectivity system across psychiatric disorders: Current status and clinical implications. *Biol. Psychiatry Glob. Open Sci.* **2**, 332–340 (2022).
86. R. Dimitrova *et al.*, Preterm birth alters the development of cortical microstructure and morphology at term-equivalent age. *Neuroimage* **243**, 118488 (2021).
87. G. Bargary, K. J. Mitchell, Synaesthesia and cortical connectivity. *Trends Neurosci.* **31**, 335–342 (2008).

88. J. Simner, V. U. Ludwig, The color of touch: A case of tactile-visual synaesthesia. *Neurocase* **18**, 167–180 (2012).
89. S. R. J. Gilissen, K. Farrow, V. Bonin, L. Arckens, Reconsidering the border between the visual and posterior parietal cortex of mice. *Cereb. Cortex.* **31**, 1675–1692 (2021).
90. L. Frangeul *et al.*, Specific activation of the paralemniscal pathway during nociception. *Eur. J. Neurosci.* **39**, 1455–1464 (2014).
91. G. Lopez-Bendito *et al.*, Tangential neuronal migration controls axon guidance: A role for neuregulin-1 in thalamocortical axon navigation. *Cell* **125**, 127–142 (2006).
92. E. C. Jacobs *et al.*, Visualization of corticofugal projections during early cortical development in a tau-GFP-transgenic mouse. *Eur. J. Neurosci.* **25**, 17–30 (2007).
93. V. Jacob *et al.*, The Matrix: A new tool for probing the whisker-to-barrel system with natural stimuli. *J. Neurosci. Methods* **189**, 65–74 (2010).